The Astrophysical Journal, 581:325–334, 2002 December 10

WATER MASERS AS TRACERS OF PROTOSTELLAR DISKS AND OUTFLOWS IN THE INTERMEDIATE-MASS STAR-FORMING REGION NGC 2071

A. C. Seth
Department of Astronomy, University of Washington, Stevens Way, Box 351580, Seattle, WA 98195;
seth@astro.washington.edu

L. J. Greenhill
Harvard-Smithsonian Center for Astrophysics, 60 Garden Street, Cambridge, MA 02138; greenhill@cfa.harvard.edu

and

B. P. Holder
Department of Physics, University of Texas at Austin, RLM 5.208, Austin, TX 78712; bholder@physics.utexas.edu
Received 2002 May 29; accepted 2002 August 16

ABSTRACT

We have mapped the water maser emission associated with the infrared centers IRS 1 and IRS 3 of the NGC 2071IR star-forming region at four epochs over ∼4 months with the Very Long Baseline Array. We detected 269 maser features with ∼1 km s^{-1} line widths and measured 30 proper motions. In each infrared center, the water maser emission appears to trace parts of a protostellar disk and collimated outflow. The disk components are ∼9 and ∼17 AU long in IRS 3 and IRS 1, respectively, and ∼2 AU wide. They are identified as disks by their compact size, elongation parallel to the direction of known IR polarization, central location in the maser maps, small internal proper motions, and proximity to λ1.3 cm continuum emission. The outflows have axes perpendicular to the disks and exhibit proper motions of up to ∼42 km s^{-1}. They are outlined by maser emission up to ∼260 AU from the protostars. The IRS 3 outflow appears to be conical on one side, while the IRS 1 outflow comprises a narrowly collimated bipolar flow surrounded by outward-facing, funnel-shaped cavities. The detection of water maser emission tracing such compact disk components and specifically conical or funnel-shaped structures is unusual. The fact that the distributions are similar in IRS 3 and IRS 1 may indicate that the two infrared centers are roughly coeval. NGC 2071IR provides a rare opportunity to resolve the structures and dynamics of disks and outflows together and to do so for two protostars that are only ∼2000 AU apart (in projection) in a deeply embedded star-forming region of intermediate luminosity.

Subject headings: H II regions — ISM: individual (NGC 2071) — ISM: jets and outflows — masers — stars: formation

On-line material: machine-readable tables

1. INTRODUCTION

The infrared cluster NGC 2071IR lies in the Lynds 1630 dark cloud in Orion at a distance of 390 pc (Anthony-Twarog 1982). The ∼30″ diameter cluster has been resolved into eight distinct near-infrared sources (Walther et al. 1993) and has a total luminosity of 520 $L_\odot$ (Butner et al. 1990), which is suggestive of intermediate-mass star formation. Snell & Bally (1986) first detected radio continuum counterparts to the IR sources, specifically IRS 1 and IRS 3, separated by 6″. While IRS 1 dominates the luminosity at near-infrared wavelengths, IRS 3 is a significant contributor at longer wavelengths (Snell & Bally 1986; Kawabe et al. 1989).

NGC 2071IR also hosts a well-studied molecular outflow that has been mapped in the emission of CO (Scoville et al. 1986; Moriarty-Schieven, Hughes, & Snell 1989; Chernin & Masson 1992), H_2 (Garden, Russell, & Burton 1990; Aspin, Sandell, & Walther 1992), CS (Zhou et al. 1991; Kitamura, Kawabe, & Ihiguro 1992), SO and SiO (Chernin & Masson 1993), HCO+ (Girart et al. 1999), and NH_3 (Zhou, Evans, & Mundy 1990). The arcsecond-resolution H_2 observations of Aspin et al. (1992) indicate that IRS 1 is the likely source for the large-scale outflow, while those of Garden et al. (1990) show elongated molecular emission associated with IRS 3 as well. Images of radio continuum emission, with resolutions as high as 0.″1, show elongated emission from thermal jets coincident with both infrared sources (Torrelles et al. 1998b; Smith & Beck 1994; Snell & Bally 1986).

Water maser emission ultimately associated with NGC 2071IR was detected even before the IR cluster and molecular outflows (Schwartz & Buhl 1975; Pankonin, Winnberg, & Booth 1977; Campbell 1978). Both IRS 1 and IRS 3 host the water maser emission (Tofani et al. 1995; Torrelles et al. 1998b), which indicates the presence of substantial columns of dust-laden, warm (300–1000 K), dense (10^8–10^{10} cm^{-3}) gas that is probably shock excited (Elitzur 1992, p. 365). Torrelles et al. (1998b) observed the masers using the Very Large Array (VLA) with resolution of 0.″1. In IRS 1, they observed a distribution of masers elongated parallel to the roughly east-west radio jet. In IRS 3, they observed a distribution more or less perpendicular to the jet and suggestive of a disk. The difference in the structure for the maser sources, supplemented by the higher extinction toward IRS 3, was inferred to indicate that IRS 3 is less evolved.

In general, the study of intermediate- and high-mass protostars is difficult because examples are hundreds of parsecs away and are contained within crowded fields. As a result, even observations with 0.″1 resolution can be confusion limited. However, long baseline interferometric observations,

with milliarcsecond resolution, can be used to map regions unambiguously (and estimate proper motions) when high brightness temperature emission, such as water maser emission, is present (see, e.g., Claussen et al. 1998; Moscadelli, Cesaroni, & Rioja 2000; Patel et al. 2000; Furuya et al. 2000; Torrelles et al. 2001; Gwinn, Moran, & Reid 1992 and references therein).

The proper-motion study of NGC 2071IR presented here concentrates on one of the closest regions of intermediate-mass star formation whose structure and dynamics we show have not been fully resolved in previous studies. In § 2, we present the observations and calibration followed by a description of how we estimated proper motions in § 3. In § 4, we discuss the compact protostellar disk and outflows found in both IRS 1 and IRS 3 and consider how these structures bear on other lower angular resolution observations of the whole infrared cluster. Conclusions are presented in § 5.

2. OBSERVATIONS AND CALIBRATION

We observed the 6_{16}–5_{23} transition of water (rest frequency 22235.080 MHz) toward NGC 2071IR with the Very Long Baseline Array (VLBA) of the NRAO[1] at four epochs in 1996 (see Table 1). A single antenna of the VLA augmented the VLBA, which provided improved sensitivity to emission extended on several milliarcsecond scales. A 16 MHz ($\sim$215 km s^{-1}) recording bandwidth, centered on $V_{\rm LSR} = 4.66$ km s^{-1}, covered the known velocity range of emission. We processed the data with the VLBA correlator, obtaining 512 spectral channels with a separation of $\sim$0.42 km s^{-1}.

The data were calibrated and images constructed using the NRAO AIPS package and standard techniques for VLBI. All four data sets were shifted to a common phase center located at the radio continuum peak of IRS 1 (Torrelles et al. 1998b) after correlation. We set the flux density scale with 30% uncertainty by template fitting total-power spectra for each antenna, where the template spectrum was itself calibrated with system temperature and published gain curves. We calibrated interferometric delay and bandpass response using observations of 0234+285, 0528+134, and NRAO 150. To remove the effects of atmospheric path length fluctuations, we self-calibrated each epoch using the strong, isolated emission at $V_{\rm LSR} = 12.75$ km s^{-1}, which originates in IRS 1. We applied this self-calibration to data for all spectral channels, created synthesis images of the IRS 1 and IRS 3 fields simultaneously, and detected emission between -2.42 and 27.92 km s^{-1} in IRS 1 and -8.69 and 27.12 km s^{-1} in IRS 3. No emission was detected in association with other infrared centers in NGC 2071IR, consistent with Torrelles et al. (1998b) and Tofani et al. (1995). The calibration error budget is dominated by a 16 cm uncertainty in the VLA station position (estimated with respect to a USNO geodetic reference frame). This causes a position uncertainty smaller than 10 μas for masers in IRS 3, which is small compared to the month-to-month $\sim$220 μas change that corresponds to a modest 5 km s^{-1} proper motion.

[1] The National Radio Astronomy Observatory is a facility of the US National Science Foundation operated under cooperative agreement by Associated Universities, Inc.

TABLE 1
JOURNAL OF 1996 VLBA OBSERVATIONS

Date	Track (hr)	Beam (mas)	P.A. (deg)	rms Noise (Jy)	Maser Spots	Maser Features
Mar 24 ...	8	0.92×0.51	-9	0.014	337	74
Jun 2	8	1.08×0.59	-1	0.016	259	67
Jul 5	8	1.03×0.57	8	0.016	310	81
Aug 3	8.5	1.36×1.26	24	0.023	168	47

3. IDENTIFICATION OF MASER FEATURES AND PROPER MOTIONS

We identified all emission components stronger than 6 times the rms noise level in the images for each spectral channel. We fitted one or more model elliptical Gaussians as needed to decompose these components into individual maser "spots," each about the same size as the interferometer beam. Position uncertainties for the spots were typically 0.05 mas. Counting all four epochs, 1074 maser spots were detected, with $\sim$40% in IRS 3 (Table 1).

We grouped the maser spots into emission features with resolved line profiles. Each feature probably represents a distinct clump of gas. Over the four epochs, we detected 269 features (Table 1). To group the spots into features, we selected spots in adjacent channels that lay within one beamwidth of each other. In ambiguous cases (e.g., a close pair of maser spots in a single channel) we selected the closest spot. For each feature, we estimated the position from the flux-weighted mean position of the contributing maser spots. The uncertainty was the greater of the formal error in the mean and the standard deviation of the spot positions.

For each maser feature detected, we also estimated spectral characteristics. We fitted Gaussian spectral line profiles to centrally peaked features comprising three or more channels. For other features, we simply adopted the flux-weighted mean velocity and maximum flux density among the contributing channels. Because the (u, v) coverage of the VLBA is flattened and sparse for sources close to the celestial equator, artifacts were common in a north-south band around bright emission. Features that lay in these bands were discounted unless they were offset in velocity. The final tally of maser features in each channel accounts typically for 50%–100% of the flux density detected in a total-power spectrum of the NGC 2071IR region (Fig. 1), which suggests that most of the maser features are small compared to the $\sim$1 mas (0.39 AU) VLBA beam and that the correct identification of imaging artifacts was largely successful. We present the maser feature line-of-sight (LOS) velocities, positions, and other characteristics for epochs 1–4 in Table 2.

After identifying features, we registered our VLBA map and the VLA map of Torrelles et al. (1998b), which corresponded to an epoch $\sim$4 months after the close of the VLBA observations. Using three persistent clumps of maser emission in IRS 1 as reference points, we aligned the maps with an estimated uncertainty of 0.″01 (corresponding primarily to uncertainty in the relative positions estimated with the VLA and proper motions between the VLBA and VLA epochs). This registration enabled us to compare our maser positions in both IRS 1 and IRS 3 with the maser and continuum positions of Torrelles et al. (1998b).

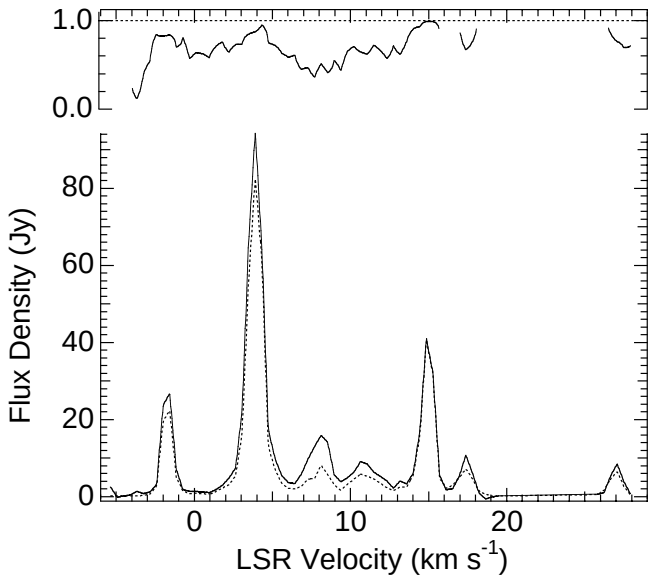

FIG. 1.—Comparison of total and imaged power for IRS 1 and IRS 3 together. *Bottom*: Total power spectrum for a roughly $\pm 1'$ field around NGC 2071IR (*solid line*) and a channel-by-channel sum of the peak flux density for each detected and fitted maser feature (*dashed line*) for 1996 March 24. *Top*: Ratio of the imaged and total power, which cannot exceed unity.

We estimated proper motions via weighted linear least-squares fits for (VLBA) features that were (1) present in at least three epochs, (2) stationary to less than 0.5 km s^{-1} along the LOS, and (3) moving in a straight line at constant velocity. To do this, first, the images for the four epochs were registered by aligning the feature at $V_{\rm LSR} = 8.76$ km s^{-1} in IRS 1 and then the 3.15 km s^{-1} feature in IRS 3. The separate registration of features within IRS 3 was necessary because of a $\sim$3 mas offset for the first epoch; feature positions for the other epochs were not offset significantly. Second, for features in IRS 1, the mean proper motion was subtracted to compensate for possible motion of the 12.75 km s^{-1} reference feature. Because positions and motions are measured in a relative sense, any plausible transverse velocity may be subtracted. Subtracting the mean proper motion is the same as assuming that IRS 1 is stationary (as sampled by the available motions). Because of the small number of motions in IRS 3, it was not possible to obtain a meaningful mean proper motion. The IRS 3 proper motions therefore include the motion of the 3.15 km s^{-1} reference feature located in the disk. The mean formal errors in the magnitude and direction of all detected motions were 9% and 5°; the medians were 3% and 1°, respectively. We present the proper motions for 30 maser features in IRS 3 and IRS 1 in Table 3.

4. DISCUSSION

The distributions of water maser emission in IRS 3 (Fig. 2) and IRS 1 (Fig. 3) are complex and difficult to model with absolute certainty. We suggest relatively simple interpretations, in the context of the current star formation paradigm. In each infrared source, the masers trace a compact protostellar disk and a collimated outflow. We suggest this model because each source contains the following:

1. A centrally located, elongated clump of maser features $\sim$9 AU (IRS 3) or $\sim$17 AU (IRS 1) long and $\sim$2 AU wide, with small internal proper motions, orientation parallel to the known direction of local IR polarization (Walther et al. 1993), and in close proximity to λ1.3 cm continuum peaks (Torrelles et al. 1998b).

2. Maser features up to $\sim$260 AU from the putative disk in which flow is oriented away from the disk and with proper motions of 17–42 km s^{-1}.

We refer to these two populations as the "disk masers" and the "peripheral masers," respectively. Figure 4 outlines the main elements of the models for IRS 3 and IRS 1.

4.1. *IRS 3*

4.1.1. *The Disk*

The central clump of water maser features in IRS 3, which we propose traces the near side of a roughly edge-on disk, is $\sim 9 \times 2$ AU in size at a position angle (P.A.) of roughly $-55°$ (Fig. 2*b*). This P.A. is consistent with the $-66°$ P.A. for 2 μm polarization observed toward IRS 3 by Walther et al. (1993), which is suggestive of scattering by material above and below the plane of an obscuring disk. In addition, the clump lies within the 1 σ error circle ($\pm$10 mas) of the λ1.3 cm emission peak of the compact radio jet (P.A. $\sim 11°$) mapped by Torrelles et al. (1998b), which is suggestive of a physical relationship between the two.

However, no compact distribution of disk masers was detected by Torrelles et al. (1998b). This is probably because the observations were limited by confusion. Nearly all of the IRS 3 maser features lie within roughly one VLA beamwidth, $\sim$0.″1 (Fig. 2*a*). Because the disk masers are not strong, they could easily be blended with stronger masers in the nearby outflow. We note as well that over the $\sim$4 months we observed, the maximum flux density of the disk masers decreased with time (Table 2). Since the Torrelles et al. observations trailed our own by another $\sim$4 months, the effects of blending may have been accentuated. Nonetheless, we note that although a rich population of disk masers was not visible, Torrelles et al. did detect four masers with velocities close to the LOS velocity of the putative disk ($\sim$4 km s^{-1}) and within one beamwidth of its location (Fig. 2).

Surprisingly, we do not detect among the disk masers a systematic velocity gradient characteristic of rotation. The mean LOS velocity of the disk masers is 4.1 km s^{-1} with a range of 3.8 km s^{-1} (Table 2). Hence, any gradient is less than 4 km s^{-1} over 9 AU (i.e., the total range in the Doppler velocities), which is suggestive of an improbably small encircled mass, $\ll 0.1\ M_\odot$. We conclude that the maser features lie at radii larger than 9 AU, where the orbital speed may be expected to be small, and that the masers sample only a confined sector on the front side of the disk. More specifically, rotating edge-on disks display gradients in LOS velocity, $\partial V_{\rm los}/\partial b = 30(M/r^3)^{1/2}$, where $V_{\rm los}$ is LOS velocity in kilometers per second, b is the impact parameter with respect to the center of the disk measured in AU, M is enclosed mass in $M_\odot$, and r is disk radius in AU. For $r = 4.5$ AU and $M = 1\ M_\odot$, the observed LOS velocity should change by $\sim$28 km s^{-1} across the IRS 3 clump, a possibility the data exclude. However, if the masers sample a small sector on the near side of a larger disk, then the upper limit on the observed gradient, a shift less than 4 km s^{-1} over $\sim$9 AU, constrains the radius of the maser region in the disk to be larger than $17M^{1/3}$ AU. Because the excitation of maser emission requires a balance of physical conditions (i.e.,

TABLE 2

WATER MASER FEATURES IN NGC 2071 IRS 1 AND IRS 3

Object	Epoch Number	Feature Number	V_{LOS} (km s^{-1})	V_{LOS} Uncertainty (km s^{-1})	Peak F_ν (Jy)	Peak F_ν Uncertainty (Jy)	East-West Offset (mas)	East-West Uncertainty (mas)	North-South Offset (mas)	North-South Offset Uncertainty (mas)	Spots in Feature	HPFW[a] (km s^{-1})	HPFW Uncertainty (km s^{-1})	Motion Number[b]
IRS 3.....	1	0	18.86	0.55	0.238	0.042	49.527	0.043	1.938	0.181	4	1.950	1.124	7
IRS 3.....	1	1	18.49	0.21	0.174	0.010	49.753	0.132	2.281	0.053	2	...	...	...
IRS 3.....	1	2	15.39	0.01	42.556	1.094	81.567	0.020	−0.891	0.066	18	0.881	0.024	...
IRS 3.....	1	3	15.22	0.21	0.320	0.018	7.851	0.042	9.846	0.029	3	0.857	0.040	...
IRS 3.....	1	4	13.17	0.21	0.095	0.014	2.609	0.176	41.282	0.173	1	...	...	...
IRS 3.....	1	5	12.75	0.21	0.122	0.014	104.294	0.036	−234.312	0.079	1	...	...	...
IRS 3.....	1	6	12.75	0.21	0.157	0.014	103.908	0.065	−236.052	0.099	1	...	...	...
IRS 3.....	1	7	11.43	0.05	1.437	0.093	2.741	0.269	40.831	0.084	7	1.520	0.113	3
IRS 3.....	1	8	10.64	0.21	0.154	0.014	1.485	0.049	40.768	0.045	1	...	...	...
IRS 3.....	1	9	7.87	0.03	1.583	0.084	0.196	0.114	43.502	0.142	7	1.264	0.077	...

NOTE.—Table 2 is published in its entirety in the electronic edition of the *Astrophysical Journal*. A portion is shown here for guidance regarding its form and content.

[a] Half-power full widths (HPFW) are quoted for features with line profiles fit to a Gaussian model.

[b] For features with measured proper motions, entries indicate the identification numbers of motions, as enumerated in Table 3.

TABLE 3

WATER MASER PROPER MOTIONS IN NGC 2071 IRS 1 AND IRS 3

Object	Motion Number	V_{LOS} (km s^{-1})	East-West Offset (mas)	North-South Offset (mas)	East-West Velocity[a] (km s^{-1})	East-West Velocity Uncertainty (km s^{-1})	North-South Velocity[a] (km s^{-1})	North-South Velocity Uncertainty (km s^{-1})	Corresponding Features[b]			
									1	2	3	4
IRS 3.....	0	24.86	−166.310	−97.542	−22.35	0.28	−35.03	0.94	...	1	0	1
IRS 3.....	1	15.50	84.444	−2.506	18.86	0.14	−10.62	0.03	2	4	7	...
IRS 3.....	2	13.36	108.188	−234.607	16.91	0.17	−16.67	0.04	...	6	12	4
IRS 3.....	3	11.64	6.196	40.722	25.46	9.22	−0.49	0.85	7	9	13	...
IRS 3.....	4	4.83	1.096	2.123	−7.94	0.20	2.21	0.07	...	13	21	8

NOTE.—Table 3 is published in its entirety in the electronic edition of the *Astrophysical Journal*. A portion is shown here for guidance regarding its form and content.

[a] Measured proper motions expressed as a velocity, assuming a distance of 390 pc.

[b] Identification numbers of maser features at each epoch (as enumerated in Table 2) that contribute to the listed proper motions.

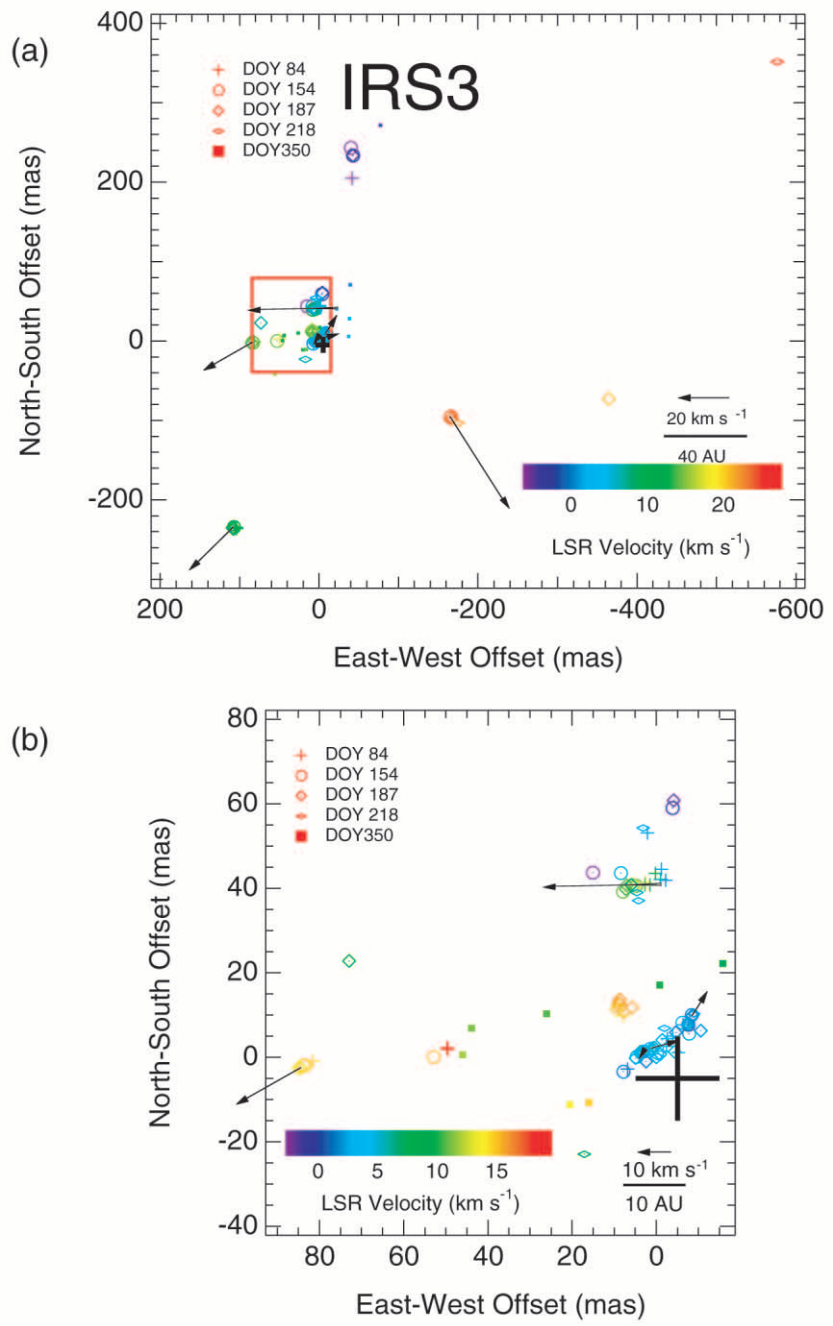

FIG. 2.—Distribution of water maser emission features in IRS 3 at four epochs in 1996 (see Table 1) and their proper motions. (*a*) All features, where color indicates Doppler velocity. Uncertainties in position are typically $\ll 0\farcs001$. Arrows indicate measured proper motions. The lengths are scaled to show the expected changes in position after 9 yr. Uncertainties in proper-motion magnitude and position angle (1 σ) are shown as tails on the arrows, where lengths indicate uncertainty in magnitude and opening angle indicates uncertainty in position angle. The uncertainties are too small to see in most cases. The black cross and filled squares indicate, respectively, the positions of the λ1.3 cm radio continuum peak and the water masers detected by Torrelles et al. (1998b) with the VLA ~4 months after the VLBA observations. The alignment of the VLA and VLBA maps is uncertain by $0\farcs01$, as reflected in the size of the cross. The map origin is $2\farcs32$ west and $5\farcs01$ north of the origin for maps of IRS 1 (see Fig. 3). The red box indicates the region plotted on an expanded scale below. (*b*) An enlargement that better shows the masers associated with the putative protostellar disk and innermost portion of the proposed outflow cone. The arrows correspond to the expected change in feature positions after 1.5 yr.

temperature and density), which probably exists only over a narrow range of radii, the disk itself could extend to larger or smaller radii. Maser action also depends on the magnitude of gradients in LOS velocity along the LOS through the disk. These gradients reach a minimum in a small sector along the front side of a disk (see, e.g., Ponomarev, Smith, & Strelnitski 1994), which is consistent with the suggested placement of maser features.

The disk masers are blueshifted by ~6 km s^{-1} (Fig. 2*b*) with respect to the 9.7 km s^{-1} systemic velocity for NGC 2071IR obtained from CO and HCO^+ observations (Moriarty-Schieven et al. 1989; Girart et al. 1999). (We will assume that the systemic velocity for both IRS 1 and IRS 3 is 9.7 km s^{-1}.) This Doppler shift is suggestive of expansion, where either (1) the disk is expanding and is warm (and dense) enough to support widespread maser action or (2)

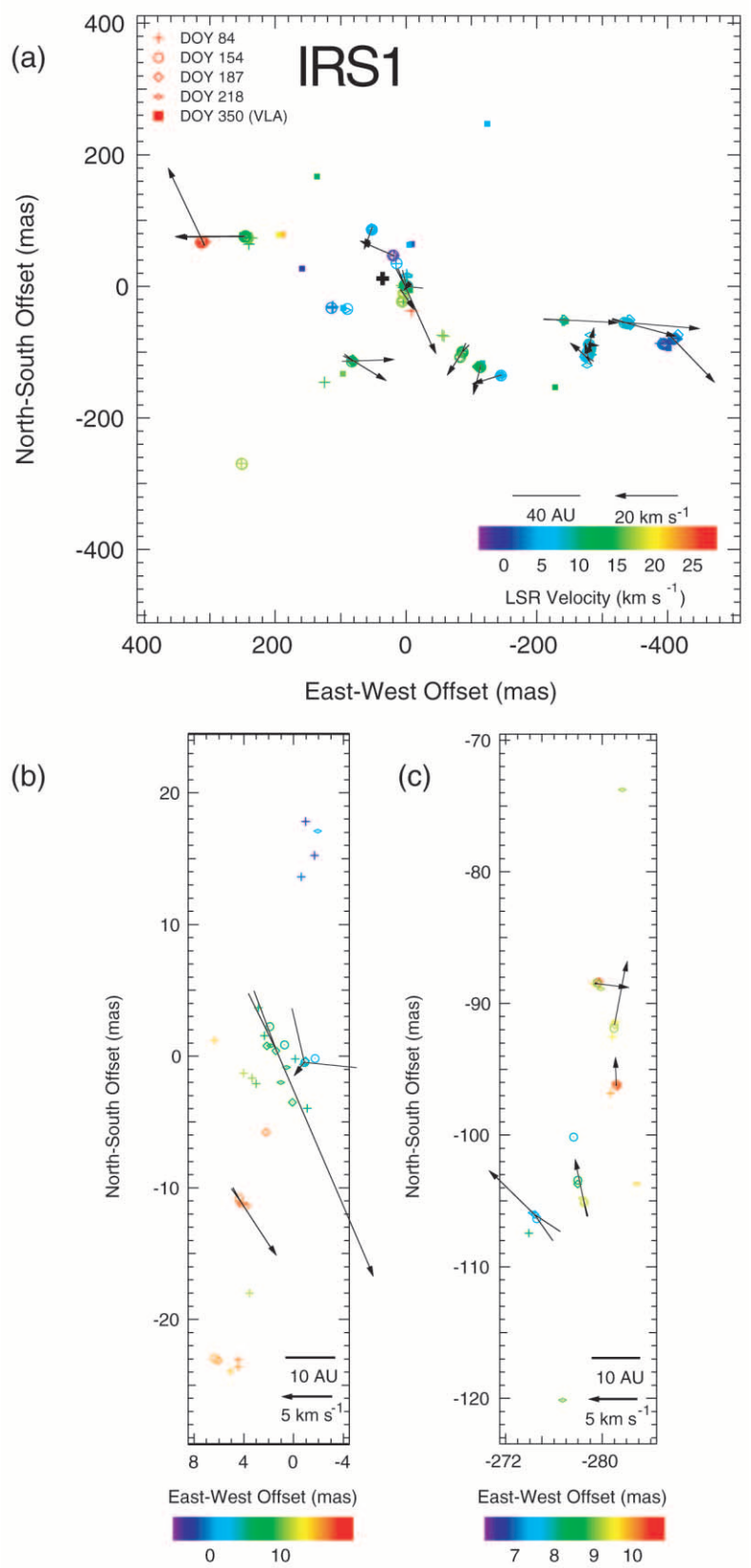

FIG. 3.—Distribution of water maser emission features in IRS 1. (*a*) All features, color coded to indicate Doppler velocity. The proper-motion arrows show the expected change in feature positions over 9 yr. The tails on the proper motions here represent 3 σ uncertainties. The λ1.3 cm continuum peak (*black cross*) and maser features (*colored squares*) measured by Torrelles et al. (1998b) with the VLA are shown with 0.″01 uncertainty in alignment relative to the VLBA maps. The origin of the map is $\alpha = 5^{h}47^{m}04^{s}.7774$, $\delta = 0°21'42''.803$ (J2000.0) with an uncertainty of 0.″05 in both directions. The red boxes indicate which fields are shown in the enlargements below. (*b*) An enlargement that better shows the masers associated with the putative protostellar disk. The arrows correspond to the expected change in feature positions after 1.5 yr. (*c*) The arc of maser features to the west that does not appear to participate in the high-speed outflow, despite its apparent proximity.

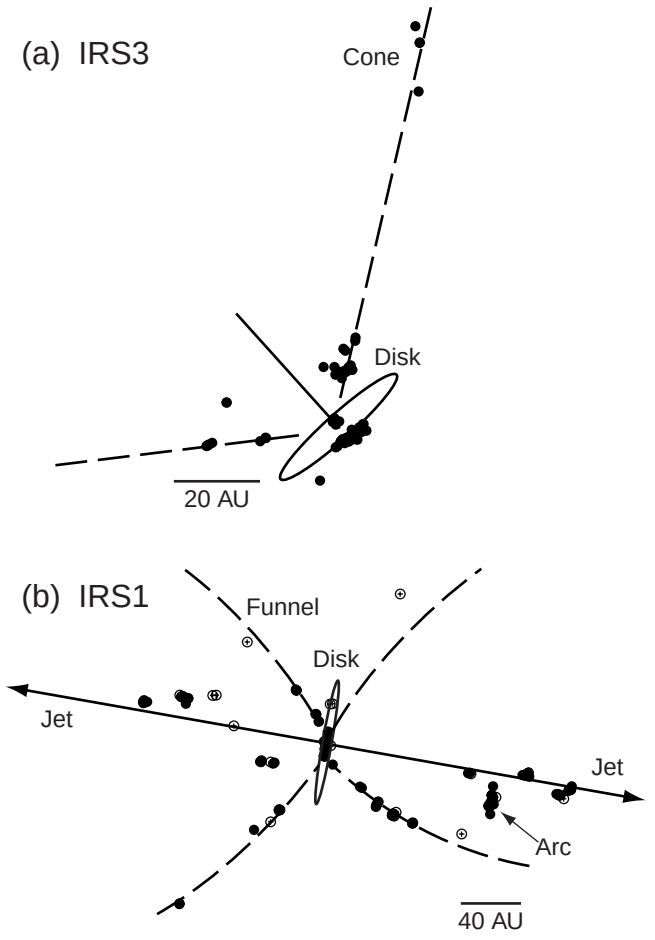

FIG. 4.—Components of our proposed models for (*a*) IRS 3 and (*b*) IRS 1.

the warm maser-laden surface layers of a cool, optically thick disk are swept outward by oblique wind-disk collision or by protostellar radiation, as could occur during photoevaporation (see, e.g., Hollenbach et al. 1994). The net blueshift of the IRS 3 disk masers is larger than their proper motion (1.8 km s^{-1}) with respect to IRS 1. This lends credibility to the suggestion that the blueshift of the IRS 3 disk masers is internal to IRS 3, e.g., expansion. (To measure the 1.8 km s^{-1} proper motion, we subtracted the mean motion of IRS 1 [see § 3] but estimated proper motions in IRS 3 without aligning the maps on the 3.15 km s^{-1} reference feature. We also used only the last three epochs.)

We note that a small clump of features with a 6 km s^{-1} redshift (relative to systemic) lies 14 mas northeast of the blueshifted disk features (Fig. 2*b*). We speculate that these could mark outflowing material on the far side of the disk. If in fact we have resolved the separation between approaching (front) and receding (back) sections of the disk, then we can constrain the disk radius (as before) and inclination together. For a 1 $M_\odot$ protostar, the radius of the maser region in the disk is larger than 16 AU, and it is tilted less than 10° from edge-on. Greater mass entails larger radii and smaller tilts. We note that in principle these blue- and redshifted maser features could also signify infall, but we favor outflow because we expect the more prominent maser emission to be on the near side of the disk, and we have inferred that the axis of the bipolar outflow is inclined slightly toward us and to the east (see next section).

4.1.2. *The Conical Outflow*

The peripheral masers are distributed irregularly over a 230 × 270 AU region (Fig. 2*a*) and exhibit proper motions of 22–42 km s^{-1} (Table 3), which are primarily directed away from the disk. These proper motions are large compared to the 5 km s^{-1} mean proper motion within the disk (Table 3). The magnitude and direction of these masers are strongly suggestive of an outflow. The mean LOS velocity of the peripheral masers is 11 km s^{-1}, in reasonable agreement with the 9.7 km s^{-1} systemic velocity. The outflow to the north and east of the disk has a mean velocity of ~8 km s^{-1} and is thus slightly blueshifted, while the much more sparsely traced outflow south and west of the disk is redshifted, with a mean velocity of ~19 km s^{-1} (Table 2).

The distribution of the outflowing masers to the north and east is similar in appearance to the limbs of an outflow cone 20–90 AU in length, which is seen most clearly in Figure 2*b* but also includes the northernmost blueshifted masers visible in Figure 2*a*. The cone has a ~110° opening angle centered on the disk minor axis (Fig. 4*a*). Based on relative LOS velocities and proper motions, it is probably inclined on the order of 10° with respect to the plane of the sky, although uncertainty in the systemic velocity of IRS 3 and sparse sampling of the outflow make the inclination difficult to estimate. The limbs of the proposed outflow cone could mark an interface between infalling and outflowing material, a scenario discussed theoretically by Delamarter, Frank, & Hartmann (2000). Such an interface would be a natural site of maser emission because of energy deposited locally by shocks (Elitzur 1992, p. 365). If the boundary layer is thin, the long velocity-coherent path lengths necessary for maser amplification will lie along the edges of the cone, close to the plane of the sky, giving the impression of limb brightening. We note a ~11 km s^{-1} difference in Doppler velocity between the two limbs of the cone. This could be attributed to the angular momentum of the infalling material. A rotation velocity on the order of 5 km s^{-1} is roughly consistent with an enclosed mass of 1 $M_\odot$ and radius of 50 AU. The sense of the Doppler shift (blueshift along the northern limb) is the same as the direction of the velocity gradient detected by Torrelles et al. (1998b), which they interpreted as a manifestation of disk rotation but which we suggest is dominated by the velocity structure of the peripheral masers.

The outflow cone can be traced to within ~20 AU of the disk (Fig. 2*b*), which suggests that collimation occurs at or within that radius. On the reverse side of the disk, the sparser appearance of the redshifted outflow is difficult to explain with certainty. Because maser action requires specific physical and dynamic conditions, the absence of emission does not necessarily imply the absence of warm dense gas, as in an outflow cone. Also, the collimating medium could be asymmetrically distributed about the disk plane, discouraging formation of a sharp cone on one side. Alternatively, a collimated redshifted outflow could exist but be obscured by gas ionized and driven outward by the IRS 3 protostar as the surrounding interstellar medium is heated. Such an uncollimated expansion could be consistent with

the two proper motions most widely separated from the disk.

4.2. *IRS 1*

4.2.1. *The Disk*

The central clump of water masers in IRS 1, which we propose traces the front side of a protostellar disk, is $\sim$17 AU long and $\sim$2 AU wide, at a P.A. of roughly -11° (Fig. 3*b*). This P.A. is similar to the -19° P.A. of the 2 μm polarization vectors observed by Walther et al. (1993), who suggest that the high polarization may be related to an obscuring disk. The peak of the compact radio continuum jet mapped by Torrelles et al. (1998b) lies $\sim$35 mas to the east and along the minor axis of the disk. Overall, the distributions of masers detected with the VLA and VLBA agree well (Fig. 3*a*), probably because IRS 1 is extended over many VLA beamwidths, which reduces the impact of the blending of maser features. However, as in IRS 3, only the VLBA detects a compact disk component. Torrelles et al. (1998b) detected only one maser in close proximity to the putative disk, about which we cannot hypothesize.

The disk masers exhibit Doppler velocities of 6–19 km s^{-1}, with the blueshifted masers lying to the north and the redshifted masers to the south (Fig. 3*b*; Table 2). This velocity gradient may be explicit evidence of rotation. Following an analysis similar to that applied to the data for IRS 3, we infer an enclosed mass of $0.6(r/10\ \mathrm{AU})^3\ M_\odot$ for an edge-on geometry. Independent estimates of mass in IRS 1 are difficult to formulate, but given that IRS 1 is the dominant source of the 520 $L_\odot$ radiated by NGC 2071IR (Butner et al. 1990), we assume a mass of a few $M_\odot$. For this mass, the implied radius of the maser emission is $\sim$20 AU, which indicates that the observed maser emission traces only a limited sector on the near side of the disk. We note that the mean velocity of the disk is 13 km s^{-1} (Table 2), a $\sim$3 km s^{-1} redshift from our assumed systemic velocity. Just as the blueshift of maser features in IRS 3 might suggest outflow coupled with rotation, this redshift in IRS 1 may imply that the material being traced by the masers is infalling. However, we treat the possible detection of infall tentatively because the redshift is small and the proper motions of disk masers (see below) are somewhat disordered, given the simple model we propose.

We have detected three proper motions in the disk, two of which have significant southward velocity components of 5 and 21 km s^{-1}(Fig. 3*b*; Table 3). The expected orbital motion is the product of the observed velocity gradient and radius, independent of enclosed mass, and may be expressed as $8(r/10\ \mathrm{AU})$ km s^{-1} toward the south. For a radius of 20 AU, we would predict a proper motion of 16 km s^{-1}, which is consistent with the observed motions. However, there is significant scatter both in the direction and magnitude of the observed motions, and better data are needed to support a complete analysis. The proper motions could be influenced by turbulence, radial flows, changing orbital velocity along the LOS, and inclination effects. Relatively few motions were measured in the disk because the lifetimes of many maser features therein were shorter than the length of the proper-motion study. In contrast, features in the surrounding outflow were longer lived. This observation should be used to guide the design of future proper-motion studies.

4.2.2. *The High-Speed Outflow and Surrounding Cavities*

The peripheral masers are distributed over a region $\sim$330 $\times$ 200 AU, elongated more or less east-west (Fig. 3*a*). The average Doppler velocity of these masers is 11 km s^{-1}, in agreement with the assumed systemic velocity of 9.7 km s^{-1}. Based on the distribution and the dynamics of maser features, we suggest that the peripheral masers trace three separate structures (Fig. 4*b*):

1. a narrow high-speed bipolar outflow oriented perpendicular to the disk elongation;
2. four arc-shaped arms extending from the disk that correspond to the limb-brightened edges of two outward facing, funnel-shaped cavities along the disk minor axis;
3. an arc of masers located 275 mas to the west and 100 mas to the south of the disk (Fig. 3*c*), which may trace a bow shock.

We discuss the high-speed outflow and cavity in this section and the arc in the next section.

The high-speed outflow appears to be narrowly collimated and oriented along a P.A. of $\sim$77° (Fig. 3*a*), perpendicular to the disk. Seven proper motions were observed in the flow with velocities ranging from 17 to 25 km s^{-1}. The western outflow is clearly blueshifted (mean Doppler velocity of 6 km s^{-1}), while the eastern outflow is redshifted. The motions are inclined from the plane of the sky by a few degrees closest to the disk, which is consistent with the assumption that the disk is edge-on. Farther out, the high-speed motions are inclined by $\sim$30°, a result of increasing Doppler shift with radius. This may be a signature of precession; however, the most inclined motions also have significantly rotated position angles suggesting that the high-speed outflow may be channeled by the surrounding medium.

When we superpose the VLBA and VLA maps of masers in IRS 1 (Fig. 3*a*), we observe four arcs that extend from the disk and appear to outline the limbs of two outward facing, funnel-shaped cavities roughly centered along the flow axis (Fig. 4*b*). The association of narrowly collimated outflow with wide-angle, possibly wind-blown, cavities is exemplified by some Herbig-Haro flows (see, e.g., Reipurth et al. 2000) and has been treated theoretically (see, e.g., Shu et al. 1994). We suggest that in IRS 1 the cavity walls represent an interface between outflowing and infalling material (as discussed earlier for the outflow cone in IRS 3), where collimation occurs at radii on the order of 10–50 AU.

We highlight two systematic patterns among the maser features. First, the northern two arcs are blueshifted by a few kilometers per second with respect to the assumed systemic velocity, while the southern arcs are redshifted by a few kilometers per second (Fig. 3*a*). The asymmetry is similar to that observed in IRS 3, although it is smaller in IRS 1. It may be attributed to rotation of infalling material, where speeds of a few kilometers per second at radii of a few tens to 100 AU are consistent with an enclosed mass of a few $M_\odot$. Second, proper motions along the southern two limbs are directed away from the flow axis and are more or less orthogonal to the limbs, which is suggestive of an expanding cavity. This is in agreement with simulations of wide-angle winds by Delamarter, Frank, & Hartmann (2000), and the evolution of the cavity might bear some similarity to that discussed by Velusamy & Langer (1998) for the B5 IRS 1 region. We note that although most of the observed proper

motions are consistent with an expanding cavity model, two motions on the northern limbs are not. If expansion has in fact been detected, then the northern motions could be a consequence of localized turbulence and shock substructure along the cavity wall (see, e.g., Gwinn et al. 1992).

4.2.3. *The Arc*

Just to the south of the high-speed outflow, about 275 mas west from the disk, we detect an arc-shaped clump of masers (Fig. 3*c*). The arc is ~8 AU in length and has 7–10 km s^{-1} Doppler velocities (Table 2). The mean proper motion of the clump is 3 km s^{-1} to the north (Table 3). However, while a number of proper motions have been measured for the clump, they are small, and the addition of small proper-motion offsets, consistent with the uncertainty in the mean proper motion of IRS 1, significantly changes their direction.

Because of its shape and proximity to the high-speed outflow, we suggest that the arc is a shock, perhaps a bow shock similar to those traced by water masers and observed by Claussen et al. (1998), Furuya et al. (2000), and Torrelles et al. (2001). Shocks are natural sites for water maser emission (Elitzur, Hollenbach, & McKee 1989; Kaufman & Neufeld 1996), and this one might indicate that the medium around the high-speed outflow is quite inhomogeneous. Alternatively, the shock may be located along the near wall of the wind-blown cavity, and its location close to the high-speed outflow is just a chance superposition. Another possibility is that the masers are associated with a second protostellar disk. At the projected separation of ~120 AU from the main disk, a space velocity of 4 km s^{-1} would be consistent with protostellar masses of ~2 $M_{\odot}$.

The 7–10 km s^{-1} Doppler velocities of the arc correspond quite well to the velocities at which the VLBA observations resolve out most of the maser emission, from which we infer that the resolved maser emission may be associated with the arc (Fig. 1). No other single structure detected in the images corresponds exclusively to this same range of velocity. The size of the maser spots in this region further support this idea—the 72 spots in the arc are on average 15% larger than those in IRS 1 as a whole. Maser emission extended along a shock front provides a natural explanation for these observations.

4.3. *Comparison to Other Observations*

There are a considerable number of observations of large-scale outflow and the IR and radio continuum emission from NGC 2071IR. The proposed disk-outflow structure for IRS 3 and IRS 1 is supported in part by (1) the near-infrared polarization observations of Walther et al. (1993), as noted previously, and (2) the morphology of high angular resolution radio continuum images (Smith & Beck 1994; Torrelles et al. 1998b). The radio continuum imaging resolves a roughly east-west structure in IRS 1, consistent with the P.A. of the high-speed flow reported here. In IRS 3, the continuum is elongated at a P.A. of 11°, which lies within the reported wide-angle outflow cone. Walther et al. (1993) and Garden et al. (1990) find a similar orientation for IRS 3 in broadband near-infrared light, while for IRS 1, the orientation is unclear.

However, the disk-outflow model proposed here for NGC 2071IR agrees less well with maps of molecular outflows on scales greater than 1000 AU. H_2 observations conducted by Aspin et al. (1992) show a bipolar outflow from IRS 1 that seems to dominate the region. It is oriented at P.A. ~ 45° with blueshifted emission to the northeast. Lower resolution millimeter-wave observations in CO, CS, and SO (Scoville et al. 1986; Moriarty-Schieven et al. 1989; Zhou et al. 1991; Chernin & Masson 1992, 1993) all show similar position angles and orientations. This is not in good agreement with the structure of the IRS 1 water masers. Aspin et al. (1992) detect no outflow from IRS 3; however, the maps of Garden et al. (1990) clearly show a low level of shocked H_2 emission associated with IRS 3 at an orientation similar to the IR and radio continuum.

The apparent differences between the outflow structures on large and small scales may be a consequence of two mechanisms. First, the ambient medium may channel the outflows, an effect seen in other systems (see, e.g., Reipurth, Raga, & Heathcote 1996; Bally & Reipurth 2001). The high-speed water maser flow in IRS 1 shows some evidence for this, executing a bend on the order of 30°. Second, it is possible that the outflow observed on large scales is created by a merging of multiple outflows in NGC 2071IR, of which the observed flows from IRS 1 and IRS 3 are but two of many.

5. CONCLUSIONS AND CLOSING COMMENTS

We have detected 269 water maser features and 30 proper motions around IRS 3 and IRS 1 in NGC 2071IR over four epochs with the VLBA. In both IR sources the maser emission appears to trace a protostellar disk and associated outflow. The disk components comprise centrally located, elongated clumps of masers, with position angles similar to those of local IR polarization and small internal proper motions. Also, the disk components lie in close proximity to peaks in the continuum emission from compact radio jets. In contrast, the outflow components are characterized by larger proper motions directed away from the putative disks. The structures of the outflows are suggestive of a one-sided conical flow (in IRS 3) and a bipolar high-speed flow surrounded by outward-facing, wide-angle cavities (in IRS 1). The limbs of the outflows may mark the interface between outflowing and rotating infalling material.

The gross similarity of structure between IRS 1 and IRS 3 indicates that they are at similar stages of development. In both IR sources, intact protostellar disks may act as reservoirs of warm dense gas that support maser action. Consequently, the inferred disks must be relatively quiescent. In both IR sources, the outflows are richly populated with water masers, which indicates that there is substantial ambient or infalling high-density material broadly distributed within ~100 AU of the protostars. Although the extinction toward IRS 3 is larger (Walther et al. 1993), the evolution of the embedded protostar therein does not seem markedly less far along.

The detection of water maser emission tracing compact disk components (10–20 AU long and ~2 AU wide), conical outflow, and wide-angle cavities is unusual. These detections have required observations with the angular resolutions characteristic of VLBI. Disks traced by water masers on larger scales have been inferred from lower angular resolution data (Shepherd & Kurtz 1999; Torrelles et al. 1997, 1998b), but confusion from blending of maser features is a risk in these cases, and confirmation requires higher angular resolution observations.

The water maser features in IRS 3 and IRS 1 sample the underlying dense gas incompletely, which limits our inferences. In order to solidify the interpretation, renewed long baseline interferometric observations are necessary. Water maser emission in regions of low- and intermediate-mass star formation is highly time variable (see, e.g., Wilking et al. 1994; Torrelles et al. 1998a), and the accumulation of maps for many epochs, registered and superposed, will better trace the underlying dense gas structures around the protostars.

We thank T. Beasley for his assistance in adjusting the data to a common phase center through reconstruction of the correlator model. We credit L. Chernin for his initiation of the NGC 2071IR proper-motion study. This work was supported in part by the Smithsonian Institution Scholarly Studies Program and Smithsonian Astrophysical Observatory R&D funds.

REFERENCES

Anthony-Twarog, B. J. 1982, AJ, 87, 1213
Aspin, C., Sandell, G., & Walther, D. M. 1992, MNRAS, 258, 684
Bally, J., & Reipurth, B. 2001, ApJ, 546, 299
Butner, H. M., Evans, N. J., Harvey, P. M., Mundy, L. G., Natta, A., & Randich, M. S. 1990, ApJ, 364, 164
Campbell, P. D. 1978, PASP, 90, 262
Chernin, L., & Masson, C. 1993, ApJ, 403, L21
Chernin, L. M., & Masson, C. R. 1992, ApJ, 396, L35
Claussen, M. J., Marvel, K. B., Wootten, A., & Wilking, B. A. 1998, ApJ, 507, L79
Delamarter, G., Frank, A., & Hartmann, L. 2000, ApJ, 530, 923
Elitzur, M. 1992, Astronomical Masers (Dordrecht: Kluwer)
Elitzur, M., Hollenbach, D. J., & McKee, C. F. 1989, ApJ, 346, 983
Furuya, R. S., Kitamura, Y., Wootten, H. A., Claussen, M. J., Saito, M., Marvel, K. B., & Kawabe, R. 2000, ApJ, 542, L135
Garden, R. P., Russell, A. P. G., & Burton, M. G. 1990, ApJ, 354, 232
Girart, J., Ho, P. T. P., Rudolph, A. L., Estalella, R., Wilner, D. J., & Chernin, L. M. 1999, ApJ, 522, 921
Gwinn, C. R., Moran, J. M., & Reid, M. J. 1992, ApJ, 393, 149
Hollenbach, D., Johnstone, D., Lizano, S., & Shu, F. 1994, ApJ, 428, 654
Kaufman, M. J., & Neufeld, D. A. 1996, ApJ, 456, 250
Kawabe, R., Kitamura, Y., Ishiguro, M., Hasegawa, T., Chicada, Y., & Okumura, S. K. 1989, in IAU Colloq. 120, Structure and Dynamics of the Interstellar Medium, ed. G. Tenorio-Tagel, M. Moles, & J. Melnick (Berlin: Springer), 254
Kitamura, Y., Kawabe, R., & Ishiguro, M. 1992, PASJ, 44, 407
Moriarty-Schieven, G. H., Hughes, V. A., & Snell, R. L. 1989, ApJ, 347, 358
Moscadelli, L., Cesaroni, R., & Rioja, M. J. 2000, A&A, 360, 663
Pankonin, V., Winnberg, A., & Booth, R. S. 1977, A&A, 58, L25
Patel, N. A., Greenhill, L. J., Herrnstein, J., Zhang, Q., Moran, J. M., Ho, P. T. P., & Goldsmith, P. F. 2000, ApJ, 538, 268
Ponomarev, V. O., Smith, H. A., & Strelnitski, V. S. 1994, ApJ, 424, 976
Reipurth, B., Raga, A. C., & Heathcote, S. 1996, A&A, 311, 989
Reipurth, B., Yu, K. C., Heathcote, S., Bally, J., & Rodriguez, L. F. 2000, AJ, 120, 1449
Schwartz, P. R., & Buhl, D. 1975, ApJ, 201, L27
Scoville, N. Z., Sargent, A. I., Sanders, D. B., Claussen, M. J., Masson, C. R., Lo, K. Y., & Phillips, T. G. 1986, ApJ, 303, 416
Shepherd, D. S., & Kurtz, S. E. 1999, ApJ, 523, 690
Shu, F., Najita, J., Ostriker, E., Wilkin, F., Ruden, S., & Lizano, S. 1994, ApJ, 429, 781
Smith, H. A., & Beck, S. C. 1994, ApJ, 420, 643
Snell, R. L., & Bally, J. 1986, ApJ, 303, 683
Tofani, G., Felli, M., Taylor, G. B., & Hunter, T. R. 1995, A&AS, 112, 299
Torrelles, J., Gómez, J., Garay, G., Rodríguez, L. F., Curiel, S., Cohen, R. J., & Ho, P. T. P. 1998a, ApJ, 509, 262
Torrelles, J., Gómez, J., Rodríguez, L. F., Curiel, S., Anglada, G., & Ho, P. T. P. 1998b, ApJ, 505, 756
Torrelles, J. M., Gomez, J. F., Rodriguez, L. F., Ho, P. T. P., Curiel, S., & Vazquez, R. 1997, ApJ, 489, 744
Torrelles, J., et al. 2001, ApJ, 560, 853
Velusamy, T., & Langer, W. D. 1998, Nature, 392, 685
Walther, D. M., Robson, E. I., Aspin, C., & Dent, W. R. F. 1993, ApJ, 418, 310
Wilking, B. A., Claussen, M. J., Benson, P. J., Myers, P. C., Terebey, S., & Wootten, A. 1994, ApJ, 431, L119
Zhou, S., Evans, N. J., Guesten, R., Mundy, L. G., & Kutner, M. L. 1991, ApJ, 372, 518
Zhou, S., Evans, N. J., & Mundy, L. G. 1990, ApJ, 355, 159